RSC Advances

ROYAL SOCIETY OF CHEMISTRY

www.rsc.org/advances

PEG-modified upconversion nanoparticles for *in vivo* optical imaging of tumors

A.N. Generalova,[a,b*] V.V. Rocheva,[a] A.V. Nechaev,[a,c] D.A. Khochenkov,[d] N.V. Sholina,[a,d] V.A. Semchishen,[a] V.P. Zubov, [b] A.V. Koroleva,[e] B.N. Chichkov [a,e] and E.V. Khaydukov [a]

[a] Institute on Laser and Information Technologies of the Russian Academy of Sciences, 140700, Shatura, Russia;

[b] M.M. Shemyakin & Yu.A. Ovchinnikov Institute of Bioorganic Chemistry of the Russian Academy of Sciences, 117997, Moscow, Russia;

[c] M.V. Lomonosov Moscow State University of Fine Chemical Technology, 119571, Moscow, Russia;

[d] Federal State Scientific Institution N.N. Blokhin Russian Cancer Research Center, 115478, Moscow, Russia;

[e] Laser Zentrum Hannover, 30419, Hannover, Germany.

* Corresponding author: Dr. Alla Generalova, e-mail: a-generalova@yandex.ru

Abstract

A novel surface modification approach of brightly luminescent upconversion nanoparticles (UCNPs) is reported. Inorganic core@shell UCNPs (core - $NaYF_4$ co-doped with Yb^{3+} and Tm^{3+} ions, shell - $NaYF_4$) were modified by intercalation with amphiphilic copolymer poly(maleic anhydride-alt-1-octadecene) followed by cross-linking with poly(ethylene glycol) diglycidyl ether (PEG-DGE). The proposed approach enables preparation of UCNPs with outmost PEG-containing layer, which provides steric stabilization and low non-specific protein adsorption. Intravenous injection of PEG-functionalized UCNPs into the mice model results in extension of the UCNP blood circulation time up to 1 hour. *In vivo* epi-luminescence imaging of mice model with Lewis lung carcinoma is ensured by high quantum yield of the modified UCNPs and passive targeting associated with efficient UCNP accumulation in solid tumors.

Key words: upconversion nanoparticles, surface functionalization, bioimaging, tumor labeling, PEG-modified UCNPs.

1. Introduction

Optical biological imaging (bioimaging) at the cellular to whole-body level has become a powerful tool that can provide high contrast and multiple visualizations of living functions [1]. Bioimaging offers unique advantages, including rapid imaging for *in situ* diagnostics and intraoperative decisions, at the same time having negligible radiation side-effects. However, only few materials can be applied for bioimaging because of the high absorbance and luminescence of endogenous tissue components, which dramatically limit deep-tissue visualization. The application of lanthanide-based upconversion nanoparticles (UCNPs) allows overcoming many problems associated with conventional imaging probes and provides visible or near-infrared emission under excitation at 980 nm wavelength.[2–4] The UCNPs are based on sequential absorption of several photons through the long lifetime and ladder-like energy levels of trivalent lanthanide ions (ytterbium, erbium or thulium), embedded in inorganic host matrix, which produce anti-Stokes luminescence. [2,3,5] The spectral band of the excitation light centered at 975 nm corresponds to the so-called biological tissue "transparency window" (650 to 1300 nm), where light penetration in tissue occurs with minimal absorption and scattering.[6] The most efficient host matrix of UCNPs is $NaYF_4$ co-doped with Yb^{3+} as a sensitizer, and Er^{3+} or Tm^{3+} as emitter. These UCNPs demonstrate unique upconversion emission under continuous wave (CW) excitation at 970-980 nm with narrow emission lines, large anti-Stokes shift of several hundred nanometers, non-photoblinking, and superior photostability.[3,7–10]

Generally, UCNPs are hydrophobic as they are capped by oleic acid (OA), dispersible only in nonpolar organic solvents, but not in an aqueous solutions or biological buffers. This fact limits their biological applications. Therefore, surface hydrophilization of UCNPs is a crucial step in an effort to create water-soluble and biocompatible UCNP probes. Surface hydrophilization can be performed using three main strategies: (1) by an exchange of capping ligand OA to modifying ligand;[11] (2) by applying surface modification exploiting properties of capping ligand;[12] or (3) by embedding of UNCPs in hydrophilic polymer particles [13]. All three strategies aim to provide the required UNCP probe collidal stability over a large pH range at different salt concentrations, insignificant variation of inherent UCNP properties, and minimize interaction with undesirable molecules, native to biological environments, which often results in nonspecific protein adsorption.[14] To date, many UCNP hydrophilization approaches using natural and synthetic polymers have been suggested.[15–17]

UCNPs have been successfully used for *in vivo* bioimaging due to the low biotissue autofluorescence and excellent probing depth [18–22]. The most common mechanism for passive nanoparticle (NP) delivery into solid tumors is the enhanced permeability and retention effect (EPR) allowing NPs to preferentially diffuse and accumulate in tumor tissues.[14,23,24] The

efficiency of the EPR-effect in NP delivery into the tumor is associated with the NP circulation half-lifetime in blood.[25,26] The high concentration of NPs in blood is required to homogeneously perfuse pathological tissue preventing NP leakage from the tumor and reducing NP accumulation in normal tissues.

It has been reported in the literature,[21] that UCNP circulation time in blood, registered by luminescent methods, was 5-10 min. UCNP probes of small hydrodynamic diameters in the range of 10-30 nm displayed an extended circulation time in blood up to 2-4 hours.[22,27] However, such small UCNPs are characterized by low quantum yield (QY) of luminescence due to the strong dependence of upconversion QY from the NP size.[28] Thus, small UCNPs in circulatory system could not be detected by luminescent methods, and other more expensive and sophisticated imaging methods, such as magnetic resonance imaging, X-ray imaging, computed tomography, and nuclear imaging were required.[15,29,30] The application of these imaging methods involved further complex synthesis steps in order to prepare UCNPs bearing magnetic or radioactive modalities.

In this paper we report a simple method of PEG-containing shell formation on UCNP surface using a low-cost commercially available cross-linker poly(ethylene glycol) diglycidyl ether (PEG-DGE)). These UCNP probes with high QY are applied for *in vivo* optical imaging of solid tumor in BDF1 mice with a Lewis lung carcinoma (LLC). The reported strategy is following: UCNPs, structured as core@shell $NaYF_4$:$Yb^{3+}$$Tm^{3+}$@$NaYF_4$ with a diameter 75±5 nm, are intercalated with an amphiphilic copolymer poly(maleic anhydride-*alt*-1-octadecene) for UCNP surface hydrophilization, then cross-linked with PEG-DGE for improving biocompatibility and circulation time in blood. PEG moiety provides good colloidal stability and low nonspecific protein adsorption in a variety of bio-environments. We examine UCNP probes for their cytotoxicity, circulation half-lifetime in blood, and passive tumor targeting in animal models. The PEG layer on the UCNP surface enables extending of UCNP blood circulation time, leading to their more effective accumulation in tumors due to the passive EPR effect. We demonstrate excellent detection sensitivity of the intravenously injected probes, targeted and efficiently accumulated in tumors, using a home-built epi-luminescence optical imaging system.

2. Experimental

2.1. Materials

Following materials were purchased from Sigma-Aldrich (USA), and used without further purification: sodium chloride, phosphate buffered saline, pH 7.0 (PBS), poly(maleic anhydride-*alt*-1-octadecene, PMAO (M_n 30000), poly(ethylene glycol) diglycidyl ether, PEG-DGE (M_n

500), 1,6-diaminohexane, coomassie brilliant blue, ortho-phosphoric acid. Ethanol, propanol-2, hexane, chloroform were of analytical grade and purchased from Sigma-Aldrich.

2.2. Methods

Optical characteristics of particles were measured using Evolution 201 spectrophotometer (Thermo Scientific, USA). Luminescence spectra were recorded by spectrofluorometer Fluorolog 3 (Horiba Jobin Yvon, France). The PL quantum yield of NPs was measured by integrating sphere (Labsphere, USA). The particle size and zeta-potential of probe in PBS buffer (pH 7.0), were measured by 90 Plus Particle Size Analyzer (Brookhaven instruments corporation, USA) at 25^{o}C using automatic function 90Plus/BI-MAS.

2.2.1. Synthesis of β-$NaYF_4$:$Yb^{3+}$$Tm^{3+}$@$NaYF_4$ NPs. The synthesis of lanthanide doped $NaYF_4$ UCNPs is based on the coordinate stabilization of yttrium, ytterbium, and thulium metal salts in a solution of oleic acid and octadecene carried out with heating in an oxygen-free atmosphere [29]. The technique of synthesis is detailed elsewhere.[17] The product of synthesis is hydrophobic monodisperse NPs (75±5 nm) with a core@shell structure (β-$NaYF_4$: 18% Yb^{3+}, 0.6% Tm^{3+}@$NaYF_4$), which form stable colloids in nonpolar organic solvents such as hexane and chloroform.

2.2.2. Intercalation of UCNPs using amphiphilic polymer followed by cross-linking with PEG-DGE. Previously described solvent evaporation technique was used to coat the synthesized UCNPs with amphiphilic polymer PMAO.[30] We used PEG-DGE with M_n 500 in order to create "core-corona" like structure. Preliminary calculations demonstrated that the *D*, distance between two terminally attached PEG chains on the surface of UCNP particle, can be 0.5 and 0.3 nm for 0.1 and 0.6 mg/ml concentration PEG-DGE, respectively (D estimated as $\sqrt{S_{PEG}}$, where S_{PEG} (nm^2) is a surface, that each PEG chain would occupy on the UCNP surface [31]). PEG chain with M_n 500 contains 2.56 Kuhn segments and the size of polymer molecule is 2.9 nm [32]. Calculated distances made it possible to use PEG-DGE with M_n 500 in order to obtain "corona" of partially folded PEG chains, uniformly coating the UCNP surface, and design "onion-like" corona of PEG.

Resulted aqueous dispersion of UCNPs-PMAO containing 0.8 mg of UCNPs was centrifuged at 13400 rpm for 10 min. The pellet was dispersed in 1 ml PBS buffer (pH 7.0) and 10 or 40 µl of 1.5% PEG-DGE aqueous solution were added. The mixture was vortexed, sonicated for 5 min, and stirred for 1 h at 95^{o}C. Thereafter the mixture was centrifuged again at 13400 rpm for 10 min with PBS buffer addition (this procedure was repeated three times to remove free cross-linker), and dispersed in 0.8 ml of PBS buffer (pH 7.0).

2.2.3. Transmission electron microscopy (TEM). The UCNPs were diluted by hexane, then sonicated and drop-casted onto a thin bar 300-mesh copper TEM grids, coated with 0.3%

pioloform. After drying in a desiccator at room temperature, the grids were imaged using a Philips CM10 TEM (Philips, Eindhoven, Netherlands).

2.2.4. Fourier-transform infrared (FTIR) spectroscopy. Pure UCNPs were thoroughly grounded and then pressed with KBr to form a tablet. The samples of UCNP modified with PMAO and PMAO-PEG-DGE with 0.1 and 0.6 mg/ml were dried using a Savant SpeedVac Concentrator (France) and prepared as potassium bromide (KBr) pellets. FTIR spectra were recorded using an FTIR spectrophotometer (Varian 3100, USA).

2.2.5. Detection of serum protein in the presence of the modified UCNPs. 100 µl 0.1% UCNPs-PMAO, UCNPs-PMAO-0.1PEG-DGE or UCNPs-PMAO-0.6 PEG-DGE in PBS (pH 7.0) were added to 500 µl of mouse serum (100-fold diluted in PBS), thoroughly vortexed, sonicated, incubated for 1 hour at 37 ^{o}C under stirring and centrifuged at 13400 rpm for 10 min. Concentration of the non-adsorbed serum proteins in supernatants was determined by Bradford's method at λ=595 nm using spectrophotometer.[33] 500 µl of mouse serum (100- fold diluted in PBS and mixed with 100 µl PBS (pH 7.0) was used as control.

2.2.6. Anti-Stokes fluorescent microscope. The blood samples were analyzed using custom-developed anti-Stokes fluorescence microscope. The AE31 fluorescence inverted microscope (Motic, China) was equipped with CW semiconductor laser at 975 nm (ATC-SD, Russia) and cooled HR sCMOS camera (Photonic Science, UK). Blood samples were analyzed at the 30 W/cm^2 laser power density. Camera exposure time was 30 sec at maximum gain. The interference filters and dichroic mirror (Semrock, USA) were used for photoluminescence (PL) and excitation signals separation.

2.2.7. Visualization system. The home-built epi-luminescent optical imaging system was used to visualize the accumulation of UCNPs at the tumor site. The test object was scanned by the CW semiconductor laser at 975 nm (ATC-SD, Russia) via 2-axis laser beam deflection unit Miniscan-07 (Raylase, Germany). The laser power density was limited by 1 W/cm^2 to prevent the overheating of biotissue. The detection of the UCNP PL signal was performed using Falcon EMCCD camera (Raptor Photonics, Northern Ireland), equipped with the F=0.95 objective. The interference filters (Semrock, USA) were placed in front of the lens, cutting the exciting laser radiation. Detailed description of used setup can be found elsewhere.[19]

2.2.8. Cytotoxicity assay. Human skin fibroblasts cultured in McCoy's medium (Life Technologies) supplemented with 10% fetal calf serum (Thermo Scientific) in culture flasks were used. The cells were cultured up to 80% monolayer density and harvested by the Versen solution (PanEco). Then, the cell suspension in the culture medium was equally split into four experimental groups of 100000 cells, and 150 µl of 0.1% NP dispersions were added to three groups. Further incubation of the cells was carried out for 24 hours at 37^0 C in the 5% CO_2

atmosphere. After incubation the cells were rinsed with PBS, resuspended in 100 μl of PBS and stained with propidium iodide (PI). Viability of the cells was analyzed using flow cytometer (BD Accuri C6). The percentage of necrotic cells was estimated on the basis of histograms given by BD Accuri C6 Software.

2.2.9. UCNP circulation in blood. 150 μl of 0.1% UNCPs in PBS (pH 7.0) modified with PMAO, PMAO with 0.1 mg/ml PEG-DGE, PMAO with 0.6mg/ml PEG-DGE were intravenously injected to Balb/c mice (average weight 23 g) through the retro-orbital sinus. No acute allergic reactions or mice death were observed at this stage. Blood samples were collected from tail vein at time intervals from 1 to 180 min after intravenously injection. The samples were analyzed using anti-Stokes fluorescent microscope. Images from four random areas were taken and calculation of NP number in all areas was made. The data were obtained from 15 mice.

2.2.10. Tumor model and passive tumor targeting. *In vivo* optical imaging of tumor with assistance of UCNPs was demonstrated on the inoculated model of epidermoid Lewis lung carcinoma (Lewis lung cancer, LLC, ATCC, CRL-1642^{TM}). 0.2 ml LLC cell suspension in DMEM (Gibco) with concentration 2×10^6 cells were inoculated subcutaneously into right flank of BDF_1 mice (C57Bl/6×DBA/2; 5-6 weeks males, received from the «Stolbovaya» laboratory animal center). The data was obtained from 15 mice (5 mice for each UCNP probe).

150 μl of 0.1% UNCPs in PBS (pH 7.0) modified with PMAO, PMAO with 0.1 mg/ml PEG-DGE, PMAO with 0.6mg/ml PEG-DGE were intravenously injected into the mice through the retro-orbital sinus when the tumor volume reached 200 mm^3. The tumor size was identical for each experimental animal group. Mice were anesthetized intraperitoneally using the mixture of Zoletil (5.0 mg/kg) and 10 μl of 2% Rometar solution (0.2 ml per mouse) 5 minutes before the injection. No acute allergic reactions or mice death were observed at this stage. The tumor site was got rid of the pelage prior visualization. The distribution of PL signal was observed *in vivo* (from the lateral or back side of mouse) and *ex vivo* (from solid tumors) using home-built visualization system.[19] The epi-luminescent images were obtained at time intervals from 1 to 180 min after injection of the NPs solution. For *ex vivo* imaging mice were sacrificed in 2 h after the UCNPs injection using drug overdose method and solid tumors were collected.

The experimental animals were housed under controlled environmental conditions (constant temperature, humidity, and a 12 h dark–light cycle) and allowed access to water and mouse chow freely. All animal experiments were evaluated and approved by the Animal and Ethics Review Committee of the N.N. Blokhin Russian Cancer Research Center.

2.2.11. Statistical analysis. Statistical analysis was performed using Student's t-test and differences were considered to be significant at $p < 0.05$.

3. Results and Discussion

3.1. Preparation of cross-linked UCNPs and their characteristics

The UCNPs ($NaYF_4$:Yb^{3+}, Tm^{3+}) were synthesized by a modified solvothermal method, as previously described [17]. Mean size of the synthesised UCNPs was evaluated as 75±5 nm, and featured the most favorable for the upconversion process in hexagonal crystal phase (Fig. 1A). The PL quantum yield of the NPs under 1 W/cm^2 intensity of 975 nm excitation was measured as 2%. The UCNPs were capped with hydrophobic oleate ligands and therefore were immiscible with aqueous solutions. We applied the hydrophilization procedure exploring hydrophobic properties of oleate as was reported.[30] Amphiphilic poly(maleic anhydride-alt-1-octadecene) (PMAO) was adsorbed to the UCNP surface due to hydrophobic interactions between the oleate ligand and the hydrocarbon chain of the polymer. Carboxylic groups, appeared as a result of the hydrolysis of anhydride functional groups of PMAO, became directed outwards (i.e. into water) rendering UCNPs hydrophilic (Fig. 1B) and providing colloidal stability. PEG, as it has been previously demonstrated, reduces nonspecific interactions with proteins through its hydrophilicity and steric repulsion effects, increasing circulation time in blood.[34] However, in order to design PEG-modified UCNPs, usually expensive functionalized PEG derivatives or PEG-containing copolymers, prepared using complicated synthetic procedures, was applied. [15] In present work we demonstrate more simple approach based on the formation of PEG-containing shell utilizing the low-cost commercially available reagent PEG-DGE.

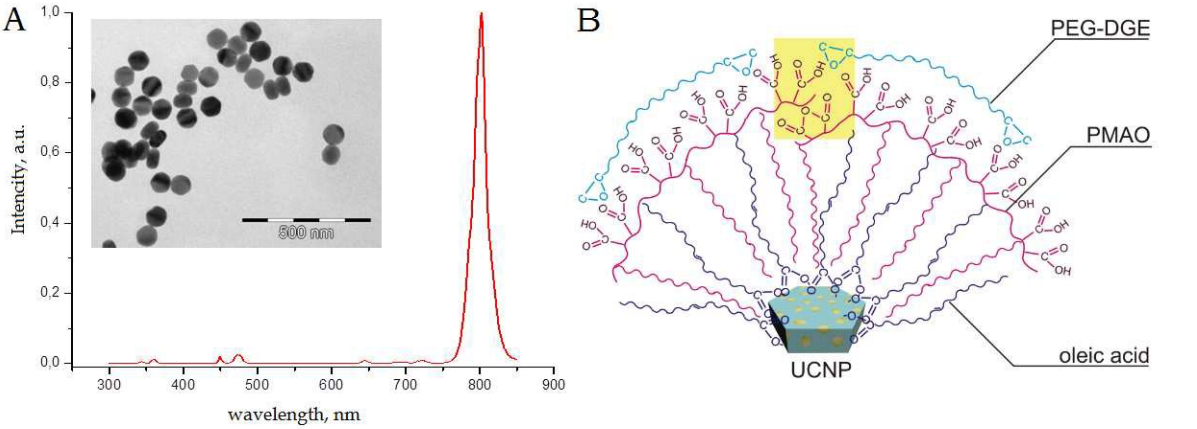

Fig. 1. TEM image and normalized photoluminescence spectrum of $NaYF_4:Yb^{3+}Tm^{3+}@NaYF_4$ upconversion NP, excited by the semiconductor laser at 975 nm with 0.5 W/cm^2 power density (A); schematic illustration of UCNP modification with poly(maleic anhydride-*alt*-1-octadecene) (PMAO) followed by cross-linking with PEG-diglycidyl ether (PEG-DGE) (B); reaction carried out on the UCNP surface, which is highlighted by yellow color in scheme B (C).

We added PEG chains on the UCNPs-PMAO surface by a cross-linking reaction with PEG-DGE using two different concentrations of PEG-DGE, 0.1 and 0.6 mg/ml, respectively. Cross-linking was carried out using the reaction between carboxyl group of PMAO and epoxy group of PEG-DGE (Fig. 1 C, reaction (1)). As a result, PEG chains were incorporated into the polymer shell on the UCNP surface. In order to confirm the reaction outcome, we analyzed Fourier-transform infrared (FTIR) spectra of the obtained UCNPs-PMAO and UCNPs-PMAO-PEG-DGE probes (Fig. 2).

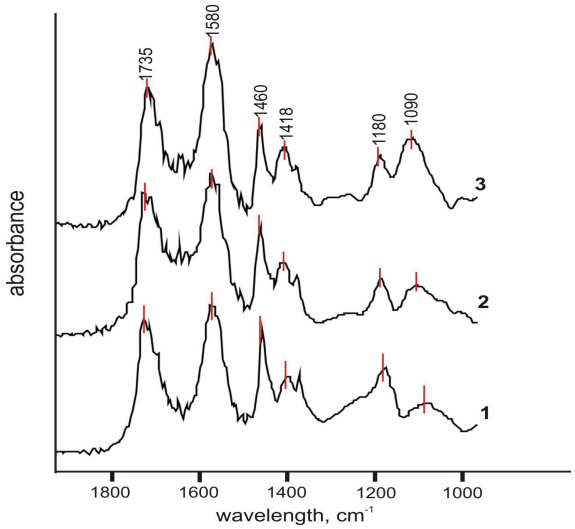

Fig. 2. FTIR-spectra of UCNPs modified with PMAO (1); PMAO with 0.1 mg/ml concentration of PEG-DGE (2); PMAO with 0.6 mg/ml concentration of PEG-DGE (3).

The spectral band at 1090 cm^{-1}, attributed to ether bond -C-O-C asymmetric stretches on spectra 2 and 3 (Fig. 2), increases with raising of PEG-DGE concentration, and that indicates the presence of $-CH_2-CH_2-O-$ groups on the UCNP surface.[35] A strong stretching vibration of -C=O (at 1735 cm^{-1}), assigned to carboxyl group, appears practically unchanged for all samples. The absorbance peak at 1580 cm^{-1}, attributed to the asymmetric -COO- stretches of carboxylic acid, as well as the band at 1418 cm^{-1}, assigned to -OH of carboxyl group, both increase at the higher PEG-DGE concentration.[36] The characteristic band of ester group C-O-C, appeared at 1180 cm-1, decreases with increasing PEG-DGE concentration.

This observation allows concluding that not only carboxyl groups take part in the cross-linking reaction, but also non-hydrolyzed maleic anhydride groups, screened by hydrophobic octadecene chains from water, take part in the cross-linking reaction due to higher

hydrophobicity of PEG-DGE compared to water. The reaction of maleic anhydride moiety with PEG-DGE, represented in Fig.1C as reaction (2), consists of two stages: first, the reaction with hydrolyzed PEG-DGE (PEG-DGE easily undergoes hydrolysis followed by ring cleavage reaction in aqueous solution) resulting in carboxyl group and ester formation; next, the reaction with epoxy groups occurring in the same way as shown in Fig.1C, reaction (1).[37] Thus, it is possible to govern the carboxyl group concentration by varying the concentration of PEG-DGE. These groups are essential in bioconjugation with target molecules and support the colloidal stability of UCNPs owing to electrostatic repulsion.

The increase of PEG-DGE concentration leads to the narrowing of UCNP size distribution and reduction of the mean UNCP size due to the compaction of polymer shell after cross-linking. It is worth noting that the zeta-potential becomes lower after cross-linking (Fig. 3A) despite the fact that PEG molecules are uncharged. This concentration-dependent decrease of zeta-potential is likely to relate to carboxyl group formation and, consequently, manifests their negative charge. The obtained cross-linked UCNPs remained colloidally stable for at least 2 months, and were unaffected by electrolytes (0.15 M NaCl and other physiological buffers), as confirmed by dynamic light scattering experiments (see SI-1).

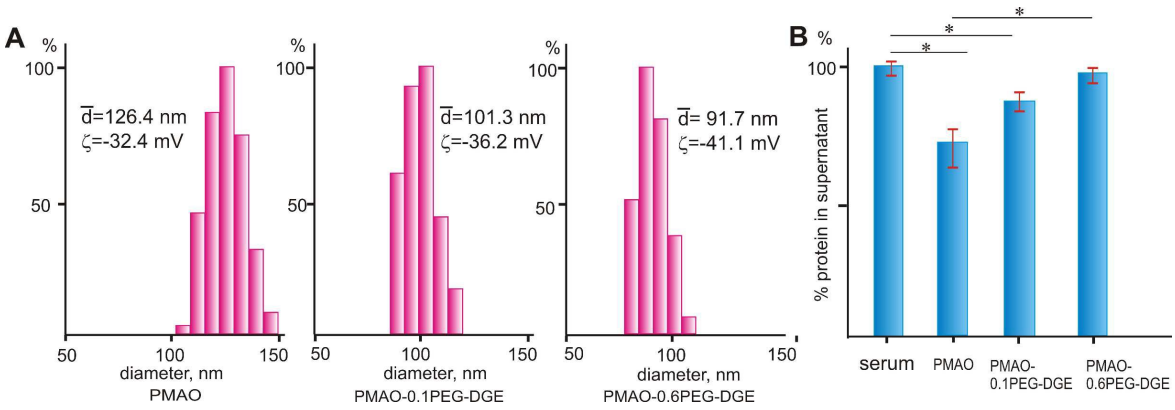

Fig. 3. Size distribution and zeta-potential of UCNPs modified with PMAO and with PMAO followed by PEG-DGE cross-linking at 0.1 and 0.6 mg/ml concentrations, PBS buffer (pH 7.0) (A); Protein amount (%) in pure serum and serum (supernatant) after incubation with UCNPs modified with PMAO and with PMAO followed by PEG-DGE cross-linking at 0.1 and 0.6 mg/ml concentrations (*: $p<0.05$) (B).

After linking with PEG molecules the polymer-coated UCNPs became stable to such a degree that their emission spectra did not change in a physiological range of pH (6 to 8) and salt conditions (0.01 to 0.5 M).

To examine nonspecific protein adsorption and stability in biological fluids, all samples of the polymer-coated UCNPs were suspended in diluted mouse serum and incubated at 37°C. Samples were precipitated, and supernatants were analyzed by using Bradford's method to

evaluate the non-adsorbed serum proteins.[33] Figure 3B demonstrates the significant decrease of protein in supernatants after incubation with UCNPs-PMAO (no cross-linker) compared to pure serum ($p<0.05$). In this case the mean diameter of UCNPs-PMAO was increased by 17 %. (147.2 nm vs 126.4 nm), and the NP aggregate formation was observed (approx. 4 %). The amount of protein in supernatant after incubation with UCNP probes containing cross-linker was higher than for UCNPs-PMAO (Fig. 3B) ($p<0.05$). Note, the higher concentration of cross-linker PEG-DGE, the higher protein concentration in supernatant and, subsequently, the lower amount of protein was adsorbed on NP surface. The size distribution of UCNPs-0.1PEG-DGE and UCNPs-0.6PEG-DGE after incubation in serum remained practically unchanged with no aggregate formation. The increase of the NP size was 14 % for UCNPs-0.1PEG-DGE (116.3 nm vs. 101.3 nm) and 11 % for UCNPs-0.6PEG-DGE (102.1 nm vs. 91.7 nm). Thus, the PEG-containing cross-linker prevents protein adsorption and provides steric stabilization of the UCNPs modified with PMAO.

3.2. Cytotoxicity of modified UCNPs

Flow cytometry assay was performed to evaluate the viability of human dermal fibroblasts incubated with the obtained UCNP probes at the 0.1 mg/ml concentration of NPs for 24 h at 37 °C. Analysis of cell viability was carried out by using flow cytofluorometer. A cellular membrane integrity marker - propidium iodide (PI) was used to label damaged cells. Intact membranes of the living cells are impermeable to PI, while PI passes through membranes of damaged or dead cells and their DNA is stained. It was shown that the viability of human dermal fibroblasts remained practically unaffected (98±2%) by the exposure to all UCNP probes at the tested concentration (see SI-2). Therefore, the cross-linker PEG-DGE did not affect the viability of tested cells, and cross-linked UCNP-PMAO may be considered safe for bioassays.

3.3. Circulation time of modified UCNPs in blood

We studied *in vivo* circulation time in blood of three UCNP probes: modified with PMAO and modified with PMAO, followed by cross-linking with PEG-DGE at two concentrations. Blood samples were collected from the tail vein at several time intervals after intravenous injection of UCNP probes to Balb/c mice. Figure 4 illustrates the UCNP distributions in collected blood samples performed by a home-built anti-Stokes fluorescence microscope. Already mentioned advantages of UCNPs, i.e. their excitation and luminescence in the ‘‘transperancy window” of biotissue, allowed detection of intense fluorescent signal from single UCNP in the samples of whole blood. Figure 5 shows the amount of UCNPs at different time intervals, obtained by direct counting UCNPs in the images. It can be seen that the UCNPs-PMAO with no cross-linker were rapidly removed from the blood circulatory system with almost 15-fold loss in first 2 minutes.

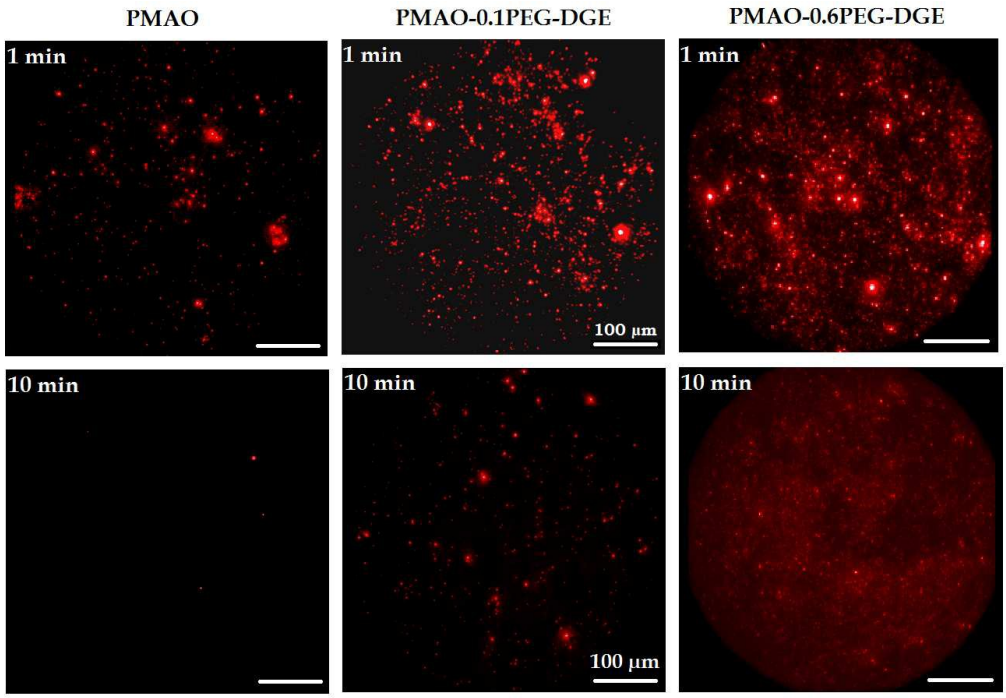

Fig. 4. Fluorescent images of mouse blood samples taken at 1 and 10 min time intervals after injection of UCNPs, modified with PMAO and with PMAO followed by PEG-DGE cross-linking at 0.1 and 0.6 mg/ml concentrations.

modified with PMAO and with PMAO followed by PEG-DGE cross-linking at 0.1 and 0.6 mg/ml concentrations.

The cross-linking of UCNPs-PMAO with 0.1 mg/ml PEG-DGE delayed the removal from circulatory system by a factor of three, while at the 0.6 mg/ml concentration of PEG-DGE, the increase of circulation time up to 60 minutes was obtained (Fig. 5). It is worth noting that individual UCNPs were detected in blood samples during the entire period of monitoring (up to 180 min).

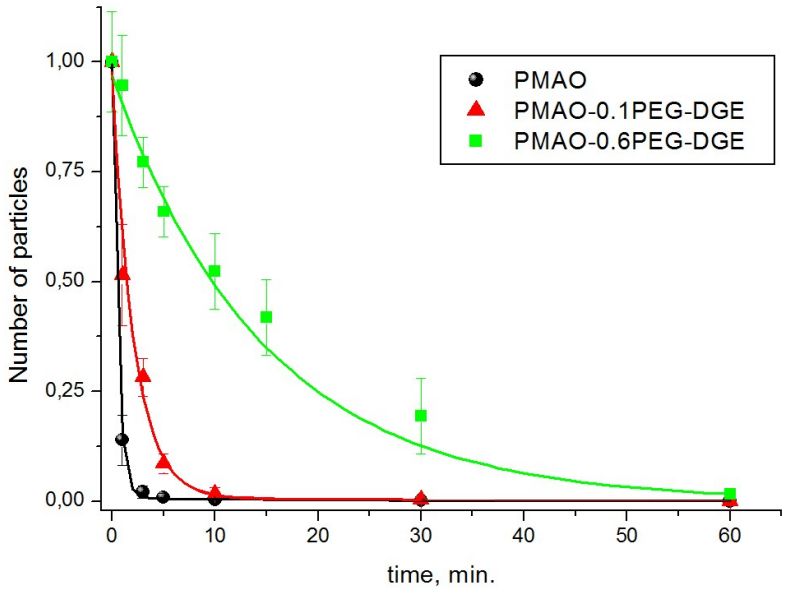

Fig. 5. Normalized dependence of the UCNP amount modified with PMAO and with PMAO followed by PEG-DGE cross-linking at concentrations of 0.1 and 0.6 mg/ml, vs. blood circulation time. The data were obtained from 15 mice (5 mice per curve).

NPs are typically removed from the blood circulation by the reticuloendothelial system – mainly by Kupffer cells in the liver and splenic macrophages, resulting in the NP accumulation in the liver and spleen.[38] It is known that the polyethylene glycol coating reduces the phagocytosis by macrophages and blood protein adsorption, prolonging the circulation lifetime in blood.[39] In our case the increased concentration of cross-linker gave rise to a growth of the PEG-containing shell and to the formation of NP surface with properties meeting the requirements for long circulation in blood.

In addition, as it was reported,[34] NPs with a negative surface charge had lower rate of cellular uptake and accumulation in the organs compared to the positively charged NPs. Moreover, in comparison with neutral charged NPs the reported functionalized NPs do not undergo aggregation. We have demonstrated that the functionalization with PEG-DGE cross-linker decreased the zeta-potential leading to significantly prolonged circulation time in blood at the maximum of PEG-DGE concentration.

3.4. Passive tumor targeting in live animals

We observed that the increase of the UCNP circulation half-lifetime in blood facilitated passive accumulation of UCNPs in the solid tumor tissues. NPs with long circulation times permeate preferentially into the tumor tissue through a tumor vasculature and are retained in the tumor due to the reduced lymphatic drainage. This process is known as the enhanced permeability and retention (EPR) effect.[24,25] The tumor growth depends considerably on angiogenesis: the formation of new blood vessels from preexisting ones for growing nutrients

supply.[40] In tumor vasculature the conventional hierarchy is absent. There are abnormally branched, non-uniform blood vessels with blind loops. One consequence of these vascular abnormalities is heterogeneity of tumor blood flow.[41] Unlike the normal blood vasculature, tumor vasculature has a high permeability through abnormal basal membrane, fewer adherent pericytes, and exhibits rapid proliferation of endothelial cells due to the production of pro-angiogenic factors in excess.[42] The pore size of tumor vessels varies from 100 nm to about 1 micron in diameter, which provides accumulation of the NPs in tumor.[43]

The lack of lymph drainage in the tumor tissue prevents NP leakage from the interstitial of solid tumors and, therefore, they are retained longer in tumor, which, together with the increased permeability of the tumor blood vessels, are responsible for the EPR effect.[44] Thus, the EPR effect enables the accumulation of larger amount of NPs in the tumor tissue than in the blood or normal tissues.

In order to visualize the polymer-coated UCNP distribution in tumor exploiting the EPR effect, we carried out an *in vivo* whole-animal imaging experiments after intravenous injection. We used custom-developed epi-luminescence imaging system to visualize the polymer-coated UCNP distribution in a LLC-bearing mice (Fig. 6).[19] UCNPs suspended in phosphate buffer saline were injected in the animal via retro-orbital sinus. No acute systemic toxicity and allergic reactions were observed.

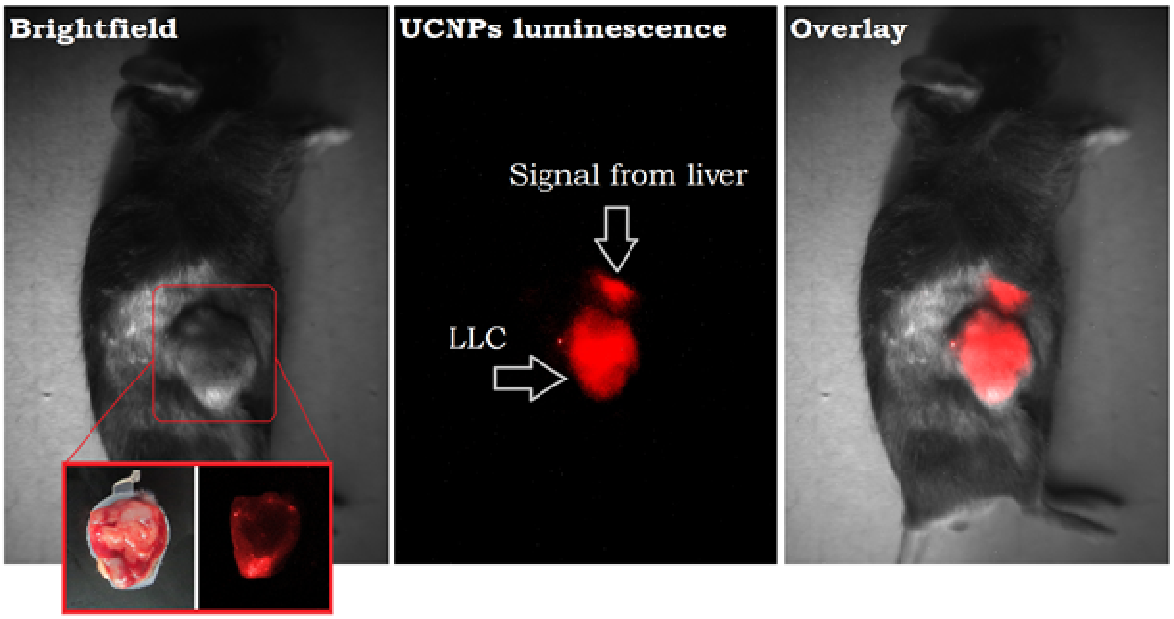

Fig. 6. Delivery of the UCNP-PMAO-0.6PEG-DGE in the LLC by the EPR-effect. *In vivo* images were taken 1 h after intravenous injection. The inset pictures are corresponding *ex vivo* photo and epi-luminescent image of tumor slice.

A rapidly vanishing signal at the venipuncture site was observed immediately after the injection. In 1 min after injection, the luminescence signal in tumor was clearly detected in 15

investigated animals. In 2 min observed luminescence of tumor decreased that was likely associated with NP redistribution towards the organs. After 5 min the luminescence signal started becoming stronger in tumor compared to other tissues and reached its maximum in 1 hour post-injection. Luminescent signal in tumor remained at the same level for 2 days. Such behavior was observed for all modified UCNPs. Figure 6 illustrates the accumulation of UCNP-PMAO-0.6PEG-DGE in the LLC tumor in 1 h after injection.

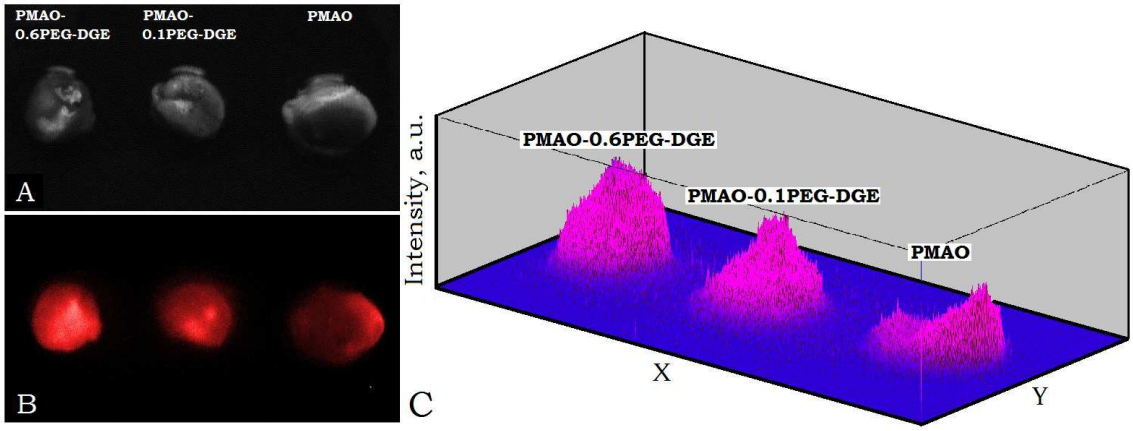

Fig. 7. *Ex vivo* bright-field (A) and epi-luminescent (B) images of solid tumors from mice injected with UNCPs-PMAO, UNCP-PMAO-0.1PEG-DGE and UNCP-PMAO-0.6PEG-DGE in saline solutions; (C) corresponding 3D plot of epi-luminescent signal.

Note, NPs preferably accumulated on the tumor periphery (Fig. 6, right inset picture), where the increased density of blood vessels, associated with the EPR effect, was observed. 3D-reconstruction of luminescent signal allows the evaluation of NP accumulation within the tumor in dependence on UCNP coating (Fig. 7). UCNPs-PMAO with PEG-DGE at maximal concentration (0.6 mg/ml) homogeneously perfused pathologic tissue in higher degree. The diameter of UCNPs-PMAO-0.6 PEG-DGE was 91.7 nm (Fig. 3A). NPs ranging from 10 to 100 nm are known to effectively penetrate and be retained in tumor.[18,45] In addition, UCNP probes have negative surface charge and PEG chains on the NP surface. These characteristics meet the requirements of NP effective delivery and passive targeting of solid tumors.[34]

4. Conclusion

Intercalation of UCNPs with amphiphilic polymer PMAO, followed by cross-linking with PEG-DGE resulted in the formation of stable colloidal aqueous suspensions of UCNPs. PEG chains on the surface of UCNPs-PMAO substantially reduced non-specific interactions with blood serum proteins through its hydrophilicity and steric repulsion effects. The functionalization of UCNPs-PMAO with PEG-DGE gave rise to significant increase of blood circulation time up to 1 hour, leading to effective targeting and accumulation of UCNPs in

tumors due to the passive EPR effect. Excellent detection sensitivity of intravenously injected PEG-containing UCNPs in the mice model with LLC tumor was demonstrated using home-built epi-luminescence imaging system.

Acknowledgements

The authors would like to acknowledge Dr. Andrey Zvyagin (Macquarie University), Prof. Evgeniya Stepanova (RCRC) and Prof. Vladislav Panchenko (ILIT RAS) for helpful discussion of the results. AVK and BNC acknowledge financial support from the Low Saxony project "Biofabrication for NIFE" and Excellence Cluster REBIRTH. Technical equipment was provided by Grant of the Government of the Russian Federation for the Support of Scientific Investigations under the Supervision of Leading Scientists Contract No. 14.B25.31.0019. This scientific work was supported by Grants RFBR No. 14-29-07241 (in part of UCNPs characterization) and RSCF No. 14-13-01421 (in part of surface modification and optical imaging).

References

1 P.N. Prasad, *Bioimaging: Principles*, 2003.

2 Q.Q. Dou, H.C. Guo and E.Ye, *Mater. Sci. Eng. C*, 2014.

3 F. Wang and X. Liu, *Chem. Soc. Rev.*, 2009, **38**, 976–989.

4 F. Wang, D. Banerjee, Y. Liu, X. Chen and X. Liu, *Analyst*, 2010, **135**, 1839–1854.

5 F. Auzel, *Chem. Rev.*, 2004, **104**, 139–173.

6 B.J. Tromberg, N. Shah, R. Lanning, A. Cerussi, J. Espinoza, T. Pham, L. Svaasand and J. Butler, *Neoplasia*, 2000, **2**, 26–40.

7 K.W. Krämer, D. Biner, G. Frei, H.U. Güdel, M.P. Hehlen and S.R. Lüthi, *Chem. Mater.*, 2004, **16**, 1244–1251.

8 L. Cheng, K. Yang, S. Zhang, M. Shao, S. Lee and Z. Liu, *Nano Res.*, 2010, **3**, 722–732.

9 G. Yi, H. Lu, S. Zhao, Y. Ge and W. Yang, *Nano Lett.*, 2004, **4**, 2191–2196.

10 M. Nyk, R. Kumar, T.Y. Ohulchanskyy, E.J. Bergey and P.N. Prasad, *Nano Lett.*, 2008, **8**, 3834–3838.

11 Q. Zhang, K. Song, J. Zhao, X. Kong, Y. Sun, X. Liu, Y. Zhang, Q. Zeng and H. Zhang, *J. Colloid Interface Sci.*, 2009, **336**, 171–175.

12 Z. Chen, H. Chen, H. Hu, M. Yu and and F. Li, *J. Am. Chem. Soc.*, 2008, **130**, 3023–3029.

13 G.S. Yi and G.M. Chow, *Chem. Mater.*, 2007, **19**, 341–343.

14 H. Kobayashi, R. Watanabe and P.L. Choyke, *Theranostics*, 2014, **4**, 81–89.

15 G. Chen, H. Qiu, P.N. Prasad and X. Chen, *Chem. Rev.*, 2014, **114**, 5161–5214.

16 Z. Wu, C. Guo, S. Liang, H. Zhang, L. Wang, H. Sun and B. Yang, *J. Mater. Chem.*, 2012, **22**, 18596.

17 E.A. Grebenik, A. Nadort, A.N. Generalova, A.V. Nechaev, V.K.A. Sreenivasan, E.V Khaydukov, V.A. Semchishen, A.P. Popov, V.I. Sokolov, A.S. Akhmanov, V.P. Zubov, D.V Klinov, V.Y. Panchenko, S.M. Deyev and A.V Zvyagin, *J. Biomed. Opt.*, 2013, **18**, 76004.

18 H. Kobayashi, N. Kosaka, M. Ogawa, N.Y. Morgan, P.D. Smith, C.B. Murray, X. Ye, J. Collins, G.A. Kumar, H. Bell and P.L. Choyke, *J. Mater. Chem.*, 2009, **19**, 6481.

19 A.N. Generalova, I.K. Kochneva, E.V Khaydukov, V.A. Semchishen, A.E. Guller, A.V. Nechaev, A.B. Shekhter, V.P. Zubov, A.V. Zvyagin and S.M. Deyev, *Nanoscale*, 2014, **7**, 1709–1717.

20 E.V. Khaydukov, V.A. Semchishen, V.N. Seminogov, V.I. Sokolov, A.P. Popov, A.V. Bykov, A.V. Nechaev, A.S. Akhmanov, V.Y. Panchenko and A.V. Zvyagin, *Laser Phys. Lett.*, 2014, **11**, 095602.

21 J. Peng, Y. Sun, L. Zhao, Y. Wu, W. Feng, Y. Gao and F. Li, *Biomaterials*, 2013, **34**, 9535–9544.

22 T. Cao, Y. Yang, Y. Sun, Y. Wu, Y. Gao, W. Feng and F. Li, *Biomaterials*, 2013, **34**, 7127–7134.

23 S.D. Perrault, C. Walkey, T. Jennings, H.C. Fischer and W.C.W. Chan, *Nano Lett.*, 2009, **9**, 1909–1915.

24 Y. Matsumura and H. Maeda, *Cancer Res.*, 1986, **46**, 6387– 6392.

25 H. Maeda, *J. Control. Release*, 2012, **164**, 138–144.

26 H. Maeda, *Adv. Enzyme Regul.*, 2001, **41**, 189–207.

27 J. Zhou, M. Yu, Y. Sun, X. Zhang, X. Zhu, Z. Wu, D. Wu and F. Li, *Biomaterials*, 2011, **32**, 1148–1156.

28 Y. Yang, Y. Sun, T. Cao, J. Peng, Y. Liu, Y. Wu, W. Feng, Y. Zhang and F. Li, *Biomaterials*, 2013, **34**, 774–783.

29 C. Lin, M.T. Berry, R. Anderson, S. Smith and P.S. May, *Chem. Mater.*, 2009, **21**, 3406–3413.

30 A.V. Guller, A.N Generalova, E.V. Petersen, A.V. Nechaev, I.A. Trusova, N.N. Landyshev, A. Nadort, E.A. Grebenik, S.M. Deyev, A.B. Shekhter and A.V. Zvyagin, *Nanoresearch*, 2015, **8**, 1546–1562.

31 C. Fang, B. Shi, Y.Y. Pei, M. H. Hong, J. Wu and H.Z. Chen, *Eur. J. Pharm. Sci.*, 2006,

27, 27–36.

32 W.C.K. Poon and D. Andelman, *Soft Condensed Matter Physics in Molecular and Cell Biology*, Taylor&Francis Group, New York London, 2006.

33 A. Darbre, *Practical Protein Chemistry—a Handbook*, Wiley, Chichester, 1986.

34 F. Alexis, E. Pridgen, L.K. Molnar and O.C. Farokhzad, *Mol. Pharm.*, 2008, **5**, 505–515.

35 M. Hesse, H. Meier and B. Zeeh, *Spectroscopic Methods in Organic Chemistry*, Georg Thieme Verlag, 1997.

36 N. Bogdan, F. Vetrone, G. a. Ozin and J. a. Capobianco, *Nano Lett.*, 2011, **11**, 835–840.

37 Z. Wang, Y.T. Cui, Z.B. Xu and J. Qu, *J. Org. Chem.*, 2008, **73**, 2270–2274.

38 A.J. Cole, A.E. David, J. Wang, C.J. Galban and V.C. Yang, *Biomaterials*, 2011, **32**, 6291–6301.

39 S.M. Moghimi, A.C. Hunter and J.C. Murray, *Pharmacol. Rev.*, 2001, **53**, 283–318.

40 R. Auerbach and W. Auerbach, in *The New Angiotherapy*, eds. T. Fan and E. Kohn, Humana Press Inc., Totowa, NJ, 2002, pp. 1–6.

41 J.W. Baish, Y. Gazit, D.A. Berk, M. Nozue, L.T. Baxter and R.K. Jain, *Microvasc. Res.*, 1996, **51**, 327–346.

42 S.K. Hobbs, W.L. Monsky, F. Yuan, W.G. Roberts, L. Griffith, V.P. Torchilin and R.K. Jain, *Proc. Natl. Acad. Sci. U. S. A.*, 1998, **95**, 4607–4612.

43 R.K. Jain, *Science*, 1996, **271**, 1079–1080.

44 A.J. Leu, D.A. Berk, A. Lymboussaki, K. Alitalo and R.K. Jain, *Cancer Res.*, 2000, 4324–4327.

45 H. Cabral, Y. Matsumoto, K. Mizuno, Q. Chen, M. Murakami, M. Kimura, Y. Terada, M. R. Kano, K. Miyazono, M. Uesaka, N. Nishiyama and K. Kataoka, *Nat. Nanotechnol.*, 2011, **6**, 815–823.

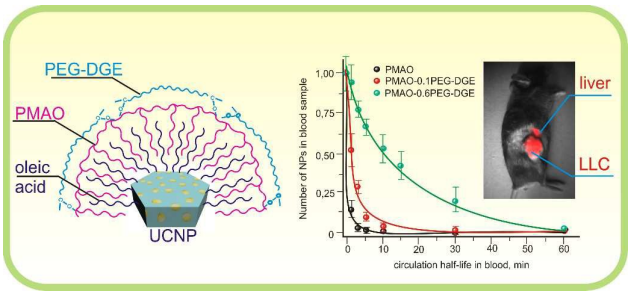

Biocompatible PEG-containing UCNPs were designed for *in vivo* passive targeting of tumor associated with UCNP efficient accumulation and tumor contrast visualization.